Available online at www.sciencedirect.com
SCIENCE DIRECT®
Corrosion Science 46 (2004) 1265–1289
CORROSION SCIENCE
www.elsevier.com/locate/corsci

Micro-cells beneath organic lacquers: a study using scanning Kelvin probe and scanning acoustic microscopy

M. Doherty, J.M. Sykes *

Department of Materials, University of Oxford, Parks Road, Oxford OX1 3PH, UK

Received 18 June 2003; accepted 8 September 2003

Abstract

The mechanism of degradation of epoxy-phenolic lacquer coated thin electro-chrome-coated mild steel (food can material) has been investigated in brine using a novel combination of experimental techniques. A scanning Kelvin probe (SKP) was used to map electrochemical potential distributions beneath the coating at several stages of exposure to 0.17 M (1% w/w) NaCl solution. An interesting sequence of events was observed, especially at defects and blisters in the lacquer. These results have been correlated with those obtained in parallel by electrochemical impedance spectroscopy (EIS), scanning acoustic microscopy (SAM) and optical microscopy. The SKP results showed coating defects to be negative (anodic) with respect to the surrounding area in the initial stages of exposure (≤ 36 h). This was followed by a gradual shift in the relative potential to values of the defect and the surrounding coated metal, with the defects becoming the cathode and the corrosion products formed in the defects becoming the cathode reactant. The reduction of red rust to magnetite was confirmed using the optical microscope. SAM revealed blisters, within which new anodes were detected by SKP.

Keywords: Corrosion; Coatings; Impedance; Cans; Blistering; Scanning acoustic microscopy; Scanning Kelvin probe

1. Introduction

Gay [1] in 1949 and Mayne in 1950 [2] devised what is now a widely accepted model of corrosion at defects in organic coatings. Mayne's model was that bare

* Corresponding author. Tel.: +44-1865-273726; fax: +44-1864-273789.
E-mail address: john.sykes@materials.ox.ac.uk (J.M. Sykes).

0010-938X/$ - see front matter © 2003 Elsevier Ltd. All rights reserved.
doi:10.1016/j.corsci.2003.09.016

metal at defects act as anode sites and coated regions supported corrosion by acting as the cathode. He proved this by galvanically coupling painted and unpainted steel coupons in seawater and demonstrating that the coated coupons were cathodic with respect to the uncoated coupons. Steinsmo and Bardal [3] recently carried out a similar experiment on coated and uncoated steel panels, coupled in seawater. They stated that the cathodic current, in this situation, is entirely limited by the ionic resistance of the coating.

In salt solutions, cathodic reduction of oxygen taking place at coated regions generates alkali by formation of hydroxyl ions (1) [4] or, in low oxygen conditions, by hydrogen evolution (2).

$$2H_2O + O_2 + 4e^- = 4OH^- \quad (1)$$

$$2H_2O + 2e^- = H_2 + 2OH^- \quad (2)$$

Schwenk [4] describes two ways in which hydroxide ions can attack coatings. Firstly, they can react directly with polar groups in the polymer, reducing adhesion. In the second, more commonly observed case; alkali metal cations from the test solution migrate to the disbonded region. They carry ionic current and combine with hydroxyl ions generated in (1), causing NaOH to accumulate at the metal surface. Analysis of blister fluid from coated mild steel samples exposed to natural seawater was carried out by Mayne [5]; the fluid was found have a pH > 12. Because of the build up of alkali, water transport through the film takes place, driven by osmosis, which generates blisters. Leng et al. [6] have proposed an alternative mechanism in which oxidative products generated in oxygen reduction, rather than alkali, attack the coating.

Crossen et al. [7] observed smooth lateral cathodic disbondment of coatings from a defect area during the early stages of immersion, which then switched to the formation of blisters ahead of the now stationary disbondment interface. The explanation suggested for this is that initial residual stresses in the coating generate shear stress at the interface sufficient to cause total loss of adhesion. After longer immersion times, water uptake in the polymer relaxes internal stresses, and there is enough residual adhesion to the substrate in areas between blisters to hold the coating in place.

Funke [8] describes a different case whereby a blister forms beneath a plugged pore. Oxygen diffuses to the edges of the blister through the intact polymer but oxygen in the region beneath the pore is consumed by oxidation of primary corrosion products in the pore from Fe(II) to Fe(III). This causes the area beneath the pore to become anodic, with the edges cathodic due to differential aeration (Fig. 1a–c); this view is supported by Geenen [9]. Wiggle [10] and other workers [11] also report that corrosion products formed at exposed areas of bare steel can subsequently plug the defect and hinder diffusion of water and oxygen.

On coated metals, corrosion initiates at defects in the coating or at sites of local coating breakdown. In the present work local behaviour around such defects has been studied as a function of time using a scanning Kelvin probe (SKP), scanning

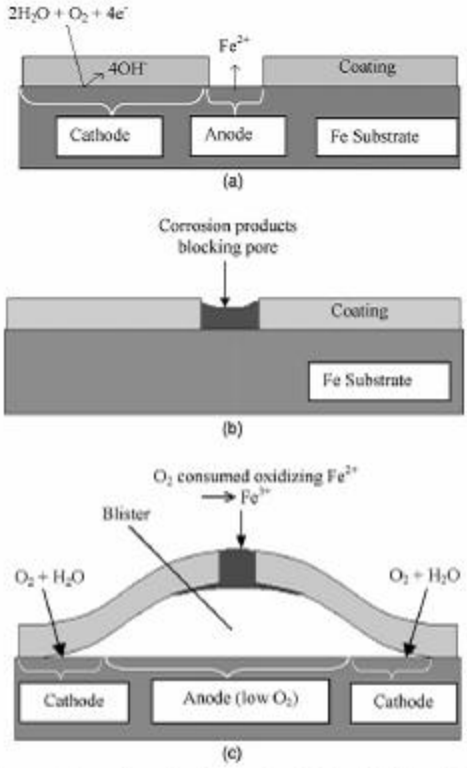

Fig. 1. Schematic representations of coated steel exposed to solution, (a) initially, (b) after pore plugging, (c) after blistering.

acoustic microscopy (SAM), optical microscopy and electrochemical impedance spectroscopy (EIS).

The SAM uses a focussed acoustic signal transmitted through an aqueous coupling medium. The acoustic waves can propagate within optically opaque solids such as organic coatings and metals. Contrast arises from differences in acoustic impedance (i.e. the product of acoustic velocity and density of the phases in the sample). The reflected echo signal is initially viewed as an A-scan (intensity vs. time delay). It is possible to identify the part of the signal corresponds to the top of the coating, the

coating/metal interface and reflections resulting from, for example, the interface of the coating and a layer of water beneath the coating. An image can be formed from any part of this echo signal by gating on the signal of interest and scanning the transducer above the sample. Thus, the presence of blisters and delamination at the metal-coating interface can be imaged, even in the early stages of coating degradation.

The SKP uses a scanned vibrating gold tip to map the volta potential (or electrochemical potential when immersed) of metals. Such measurements can be performed through organic coatings provided there is no Donnan or other potential difference across the film. This allows potential measurements of corrosion processes occurring in blisters and delaminated areas as well as at defects. This technique was used to study corrosion around a defect as a function of time to inform a mechanistic description of the process. The work detailed here shows that for lacquer on electro-chrome-coated steel (a chromium/chromium oxide treated steel sheet, used in packaging), the observed behaviour was very different to that described previously.

2. Experimental

A heat cured commercial epoxy-phenolic lacquer was roll-coated in one pass to a thickness of 7 μm on to electro-chrome-coated steel (ECCS) canning strip and heat cured for 10 min at 205 °C. Sheet was formed into DRD (drawn, re-drawn) cans (73 mm diameter, 57 mm height) following curing. Sections (ca. 2 cm^2) were cut from the walls and base of the can, as well as from unformed sheet, for exposure to test solution. A wire was soldered to each sample to facilitate EIS and SKP measurements, and the back, exposed wire and cut edges of the samples were masked using hot 4:1 beeswax/colophony mixture.

The samples were immersed in naturally aerated 0.17 M NaCl solution (or in one case 0.1 M citric acid) at room temperature and examined periodically using EIS, SKP, SAM and an optical microscope. EIS measurements were made at regular intervals using an ACM Instruments GILL AC potentiostat with paint buffer interface. The cell used a three-electrode arrangement, with a saturated calomel reference electrode (SCE) and a platinised titanium counter electrode. Impedance was measured between 30 kHz and 0.1 Hz under potential control at the rest potential, using an excitation amplitude of 20 mV. The results were fitted to an equivalent circuit using Echem Software (ZsimpWin version 2.2). The data were typically fitted to the equivalent circuit shown in Fig. 2a or to the equivalent circuit shown in Fig. 2b if a Warburg impedance was observed at low frequencies (characterised by a 45° line on the Nyquist plot). A Warburg impedance response is due to diffusion and is displayed as W, a constant phase element with $n = 0.5$.

SAM images were taken using a KSI WINSAM 200 instrument operating with a 150 MHz acoustic lens using distilled water as the coupling medium. In this work, the signal was gated to form an image of the coating/metal interface so that accu-

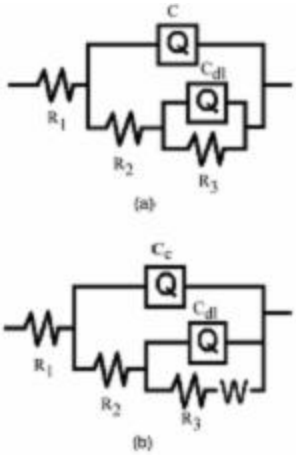

Fig. 2. (a) Two time-constant equivalent circuit, used for fitting EIS data, (b) two time-constant equivalent circuit with Warburg impedance element.

mulation of water at this interface could be observed. The operating principles are outlined in more detail elsewhere [12].

The Kelvin probe used was a KP Technology SKP, fitted with a flat 500 μm gold tip. Samples were removed from the test solution and blotted before examination. A humidity enclosure was used during the SKP scans (RH ~ 80%) to ensure the samples did not dry out fully and cause problems of charging. The instrument was operated such that a constant mean sample-tip separation of 212 ± 2 μm was maintained throughout, thus eliminating spacing-dependence errors observed by other workers [13]. The tip was set to vibrate at the resonant frequency of 59.5 Hz; with an amplitude of 168 μm. Measurements were taken using a sample backing voltage, V_b, in the range ± 5000 mV. The SKP data were plotted using Microcal Origin 7.0. A thorough description of the instrument and explanation of the tracking system is given in [14].

3. Results

Fig. 3 is a plot from impedance measurements of pore resistance, R_p, over time for a sample of lacquered ECCS immersed in aerated NaCl solution. It can be seen that R_p fell rapidly during the first 5 h before stabilising at a value of about 10^5 $\Omega\,cm^2$.

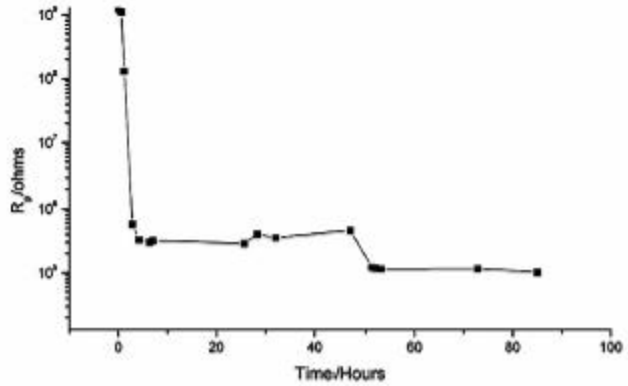

Fig. 3. Plot showing R_p over time for coated sample in 1% NaCl solution.

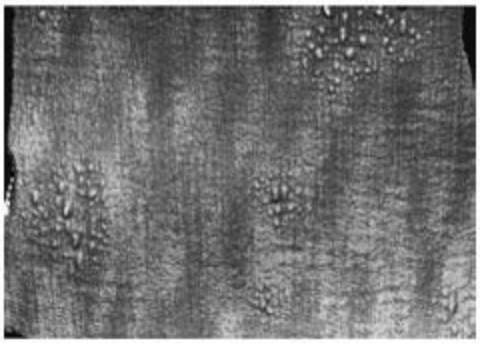

Fig. 4. SAM micrograph of coated ECCS sample after 48 h exposure to 1% NaCl solution.

After 48 h corrosion became visible on the surface of the sample and blisters were observed using SAM (Fig. 4). Once corrosion had initiated, the SKP was used to map the corrosion spot and surrounding area. Fig. 5 is a potential map acquired after 55 h that shows, unexpectedly, that the central defect is cathodic (more positive) to the surrounding area. This result was surprising because corrosion products could be seen in the pore. All maps are based on 625 measurements and are presented in terms of relative potentials with white the most negative and black the most positive, with contour lines at 50 mV intervals.

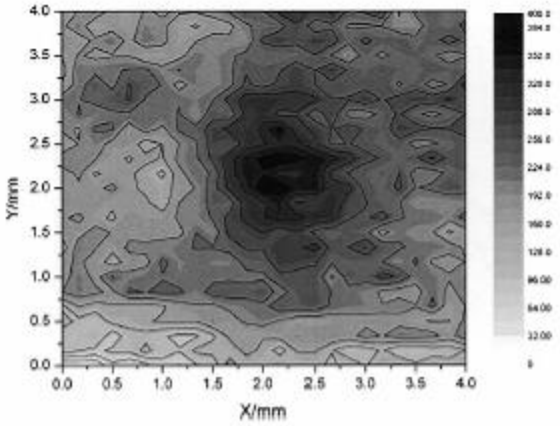

Fig. 5. Relative potential map of defect and surrounding area, taken with SKP.

A second sample of lacquered TFS was prepared as before. In order to initiate corrosion at a known site, a circular defect was made in the centre of the sample with a scalpel (1 mm in diameter). The defect and surrounding area were investigated using the SKP after various times of exposure. Fig. 6a–d show potential maps of the sample over time. There does not appear to be a sudden discontinuity in potential at the edge of the coating, from which we deduce that the potentials measured are not affected by any potential difference across the coating. This sequence shows that the defect was at first anodic, as expected, giving the lowest potential. However, the defect was only anodic for a short time (between 40 and 180 min). After 180 min, the defect was undetectable to the SKP, but the scan taken after 52 h showed the defect emerging as a weak cathode site and Fig. 6d shows that this had become much stronger after 94 h (as with the previous sample).

Interpretation of these maps requires care. The most negative potential will not correspond to the largest anodic currents (polarising an anode upwards increases the current density), nor the most positive areas the largest cathodic current (by a similar argument). The potential gradient at any point indicates the direction and magnitude of the current flow across the surface (though it should be borne in mind that Stratmann [16] has identified steep potential gradients in SKP profiles as the limit of cathodic disbonding). Only by making assumptions about the thickness of the electrolyte layer beneath the lacquer and its resistivity (which may not be uniform), can any quantitative conclusions be reached. We will show how anodic and cathodic currents can be visualised from the SKP scans in a further paper [17].

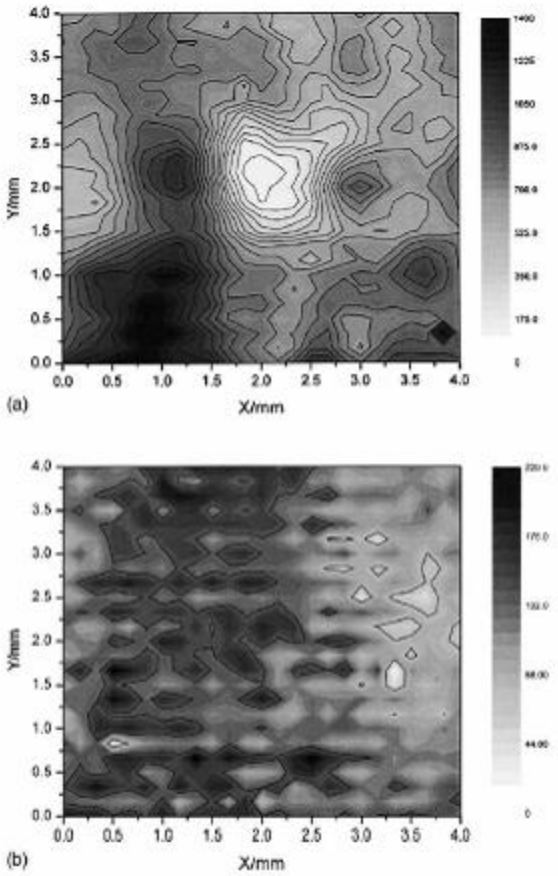

Fig. 6. Maps of relative potential (ΔE/mV) taken at various exposure times: (a) 40 min, (b) 180 min, (c) 52 h, (d) 94 h.

Fig. 7a–e shows a series of SKP images of a corrosion site in another sample with corresponding optical micrographs and SAM images. This sample was from a section that had undergone a degree of strain in the drawing process.

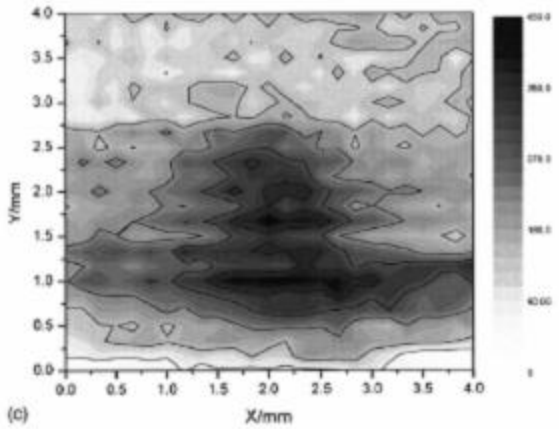

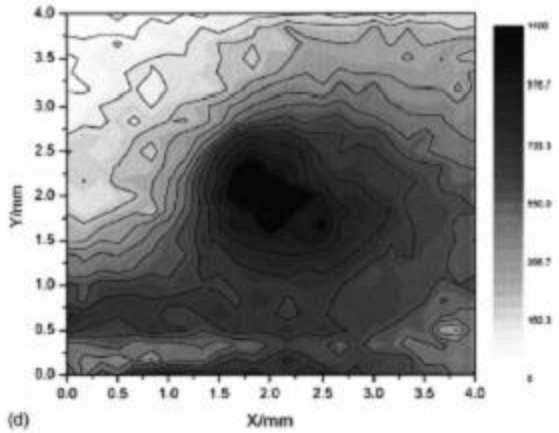

Fig. 6 (*continued*)

The optical micrograph taken after 24 h (Fig. 7a(ii)) shows red rust had formed at the defect, so corrosion had already begun. The SAM image shows the presence of blisters around the defect. The SKP scan detects the defect and the surrounding blisters as anodic regions.

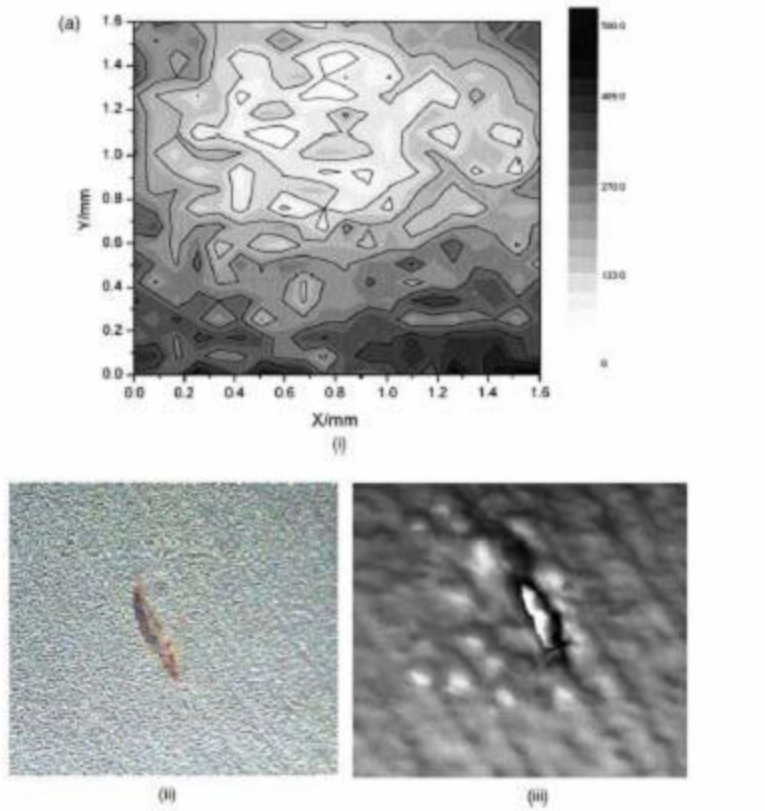

Fig. 7. Concurrent SKP (i), Optical (ii) and SAM (iii), results at various times of exposure to 1% NaCl solution; (a) 24 h, (b) 48 h, (c) 96 h, (d) 168 h, (e) 212 h.

The SKP scan after 48 h exposure (Fig. 7b) shows the corrosion site had become cathodic. This switch was initiated, we believe, as a result of plugging of the defect by corrosion products. The blister to the right of the initial corrosion site had now become anodic. This new anode was observed more clearly in the optical micrograph taken after 96 h (Fig. 7c), where red rust was observed in the large blister. The cathode site (the site of the original defect) was by this stage larger and black in colour, due, we believe, to further reduction of red rust to magnetite.

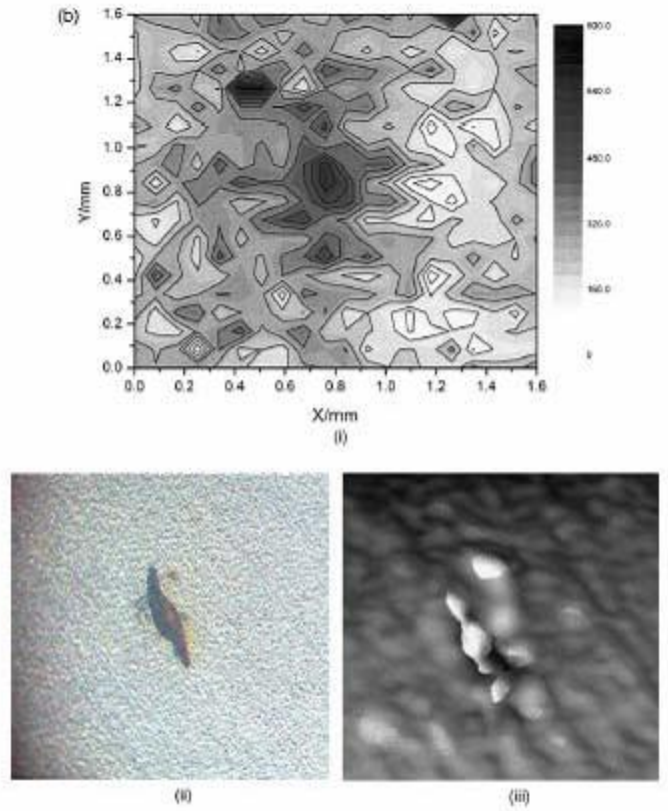

Fig. 7 (*continued*)

The anodic blister continued to fill with red rust and was still observed after 168 h (Fig. 7d); the original defect site remained cathodic. After 212 h (Fig. 7e), the optical micrograph shows that much of the red rust observed in this blister was also turning black. This demonstrates reduction of these corrosion products was now beginning. The SKP scan now measures cathodic potentials in this region too.

Fig. 8 shows the variation of pore resistance over exposure time, gathered from EIS results. The resistance falls to a low value in an hour.

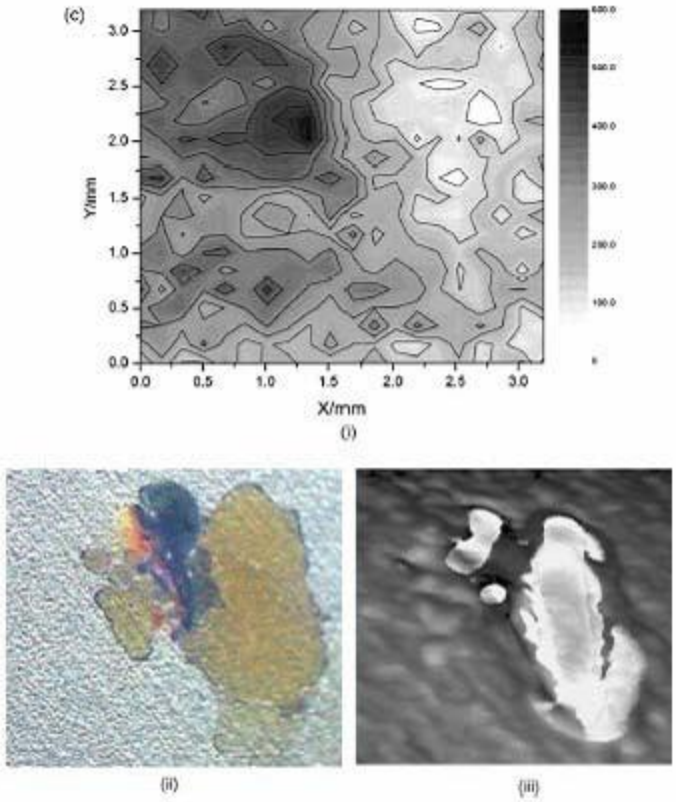

Fig. 7 (*continued*)

A further sample of the same lacquer-substrate system was exposed to NaCl solution as before. This sample had been subjected to severe non-uniform deformation during forming of the can. This experiment aimed to investigate the effect of removing corrosion products after the anode–cathode switch had taken place by exposure to citric acid. Corrosion initiated in a region of high strain and was observed 3 h after exposure.

The corrosion spot was anodic after 3 h exposure (Fig. 9a) and at 60 h (Fig. 9b) the optical microscope image showed red rust at this site. The corresponding SAM

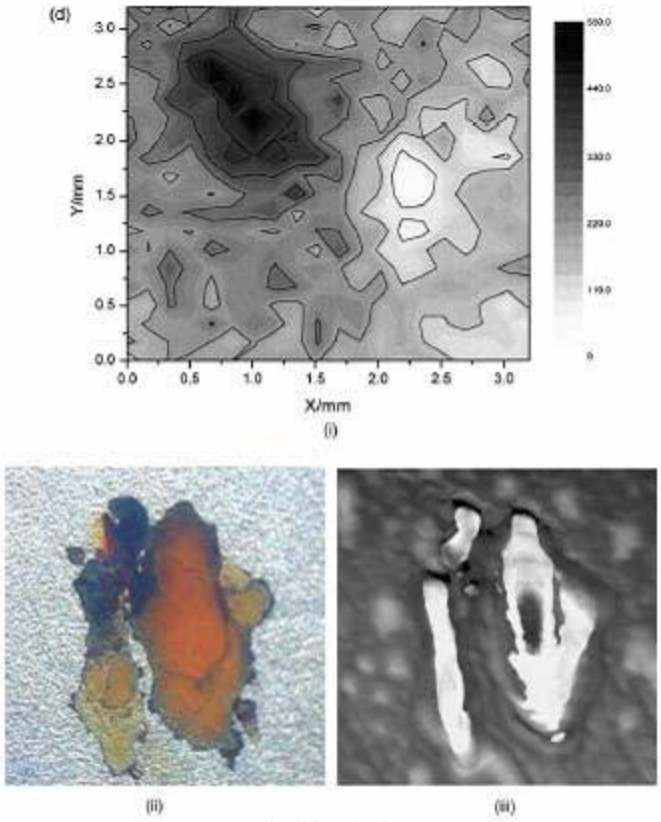

Fig. 7 (*continued*)

image shows the familiar presence of blisters surrounding the defect. The SKP scan shows that both the blisters and defect were anodic with respect to surrounding areas. A cathode site positioned out of view may have been driving the corrosion process at this stage. The SAM images show that many blisters had formed on the sample and were no longer confined to the area immediately surrounding the defect. These blisters were aligned in the drawing direction.

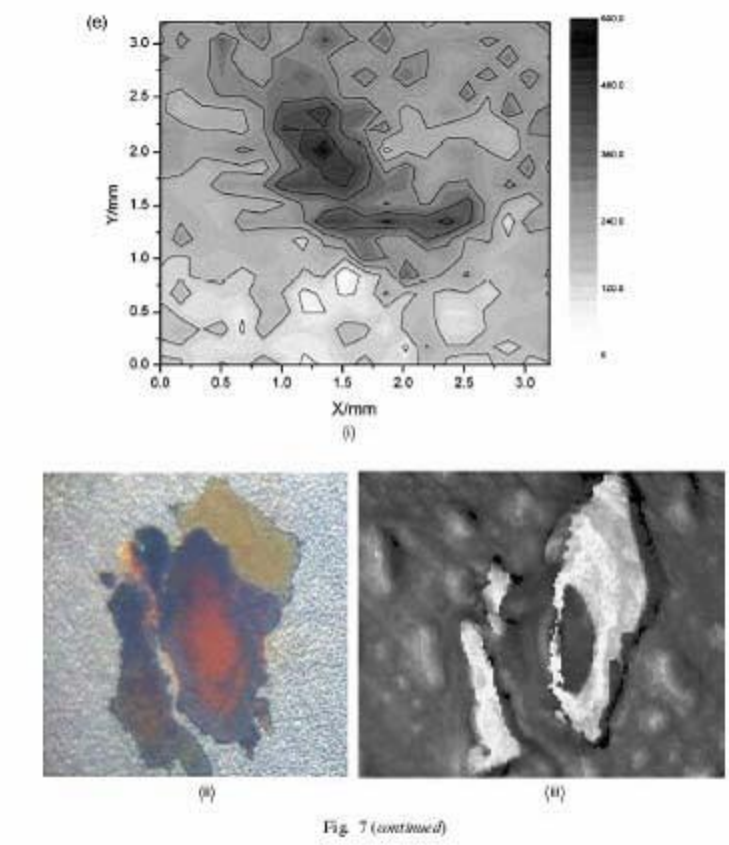

Fig. 7 (*continued*)

After 168 h (Fig. 9c) cathodic activity was still observed above the corrosion site. The original anode had died away and was now seen as a weak cathode area. The optical image showed considerable under-film corrosion around the initial corrosion site. This appeared to have become blocked by rust, and switched to be the cathode. At 215 h (Fig. 9d) the defect area was more strongly cathodic; the original cathode site above had died out.

After 220 h the sample was transferred to 0.1 M citric acid, as in previous work [16]. Citric acid forms complexes with iron corrosion products, so in the optical

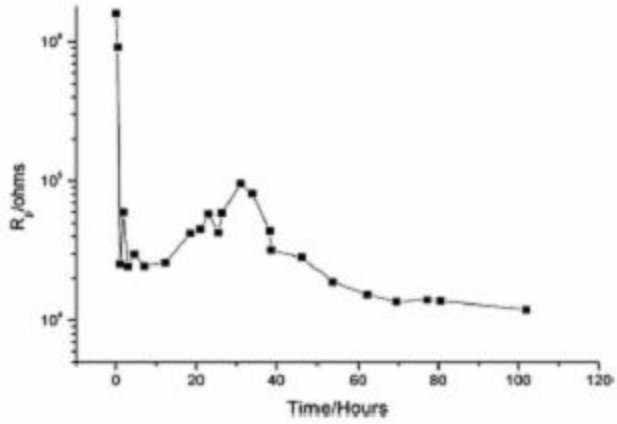

Fig. 8. Plot of variation in pore resistance (R_p) over time, plotted from EIS data.

image taken at 238 h (Fig. 9e) we observed that the magnetite beneath the coating had been removed. However, some corrosion products were still seen in the defect and the SKP scan shows the defect region has remained cathodic. After a further 31 h in citric acid (Fig. 9f), the pore plug was partly removed, and the defect had become anodic again, as expected.

The optical image taken after 333 h (Fig. 9g) shows the defect was, by this stage, fully unplugged, exposing bare metal. The SKP scan shows the defect was, as at the beginning of exposure, strongly anodic.

Some EIS results for the sample, over time, are shown in Fig. 10. The Nyquist plot taken after 5 h (Fig. 10a) shows two well-separated semi circles. The high frequency semi-circle corresponds to the contribution of the pore resistance (R_p) and coating capacitance (C_C), and the low frequency portion shows the impedance response of the corrosion reaction taking place in the base of the pore (a parallel combination of charge transfer resistance (R_{CT}) and double-layer capacitance (C_{DL})). When pore plugging began to occur, the low frequency semi-circle was partly masked out by Warburg impedance (Fig. 10b—taken after 20 h). This shows that the corrosion reaction was hindered by mass transport to the corrosion site. After 170 h (Fig. 10c), the effect is more pronounced, with the whole of the low frequency semi-circle masked out by the Warburg line.

Fig. 10d shows the Nyquist plot 50 h after the sample was immersed in citric acid; the Warburg impedance had disappeared, showing the charge transfer reaction was no longer affected by diffusion.

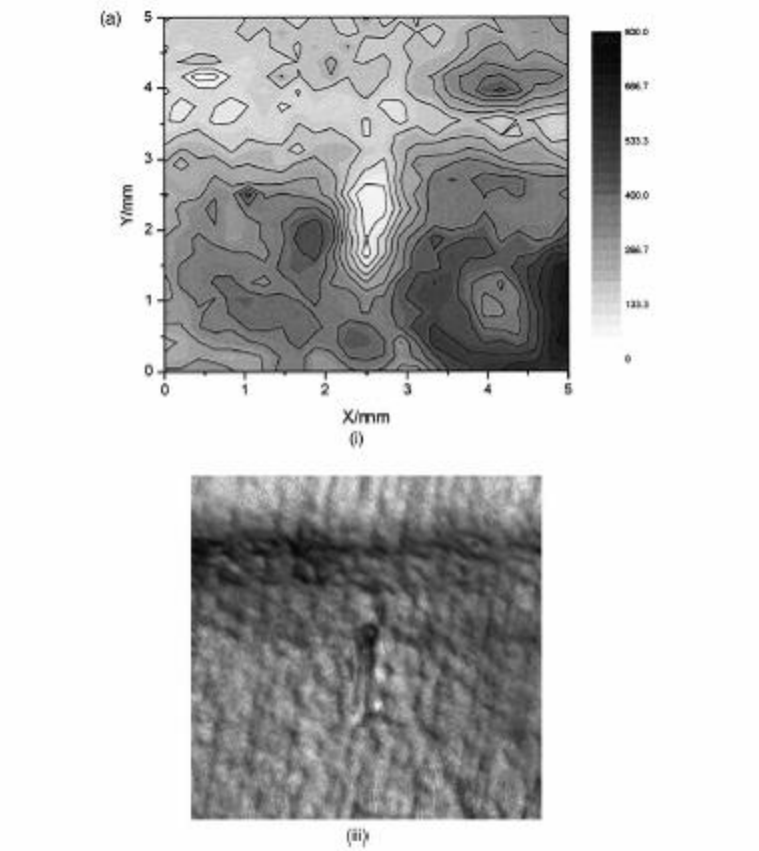

Fig. 9. Concurrent SKP (i), Optical (ii) and SAM (iii), results at various times of exposure to 1% NaCl solution, followed by 0.1 M citric acid solution; (a) 3 h [no optical image, as corrosion is not yet apparent], (b) 60 h, (c) 168 h, (d) 215 h, (e) 238 h total; 18 h in citric acid, (f) 269 h total; 49 h in citric acid, (g) 333 h total; 113 h in citric acid.

4. Discussion

A mechanism for the observed processes is proposed as follows: Initially the exposed metal at the defect was attacked and oxygen reduction took place underneath

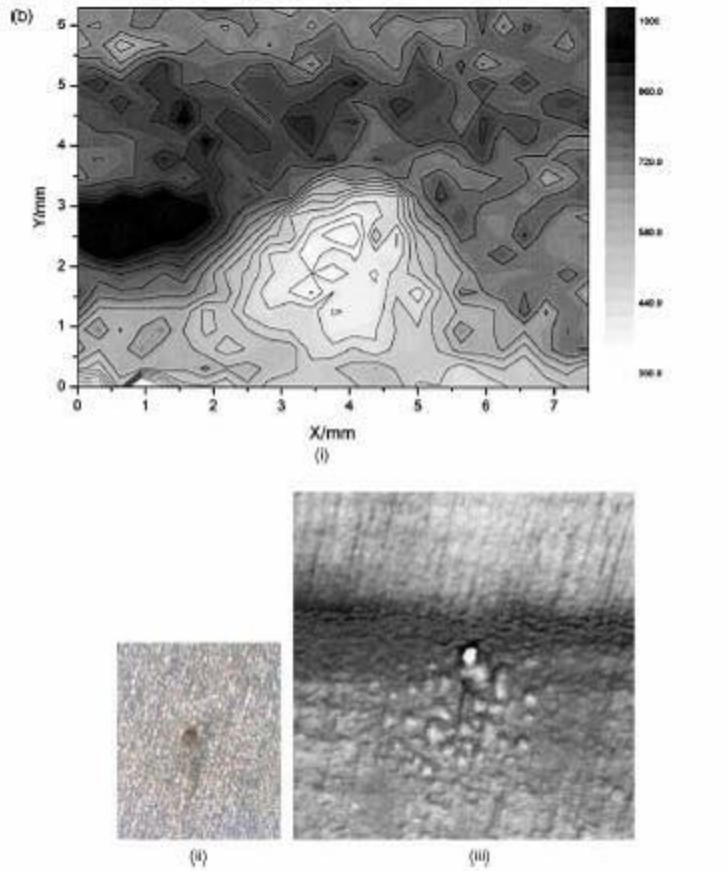

Fig. 9 (*continued*)

the film at cathode sites, in keeping with the generally accepted model. After a sufficient time, the exposed area becomes covered by precipitation of insoluble corrosion products that are converted to FeOOH by reaction with oxygen in solution, thus hindering access of oxygen to the bare metal. The defect is plugged. After this, contact between the rust and the metal surface initiates reduction of the corrosion products driven by anodic attack of any exposed regions of bare iron, as seen

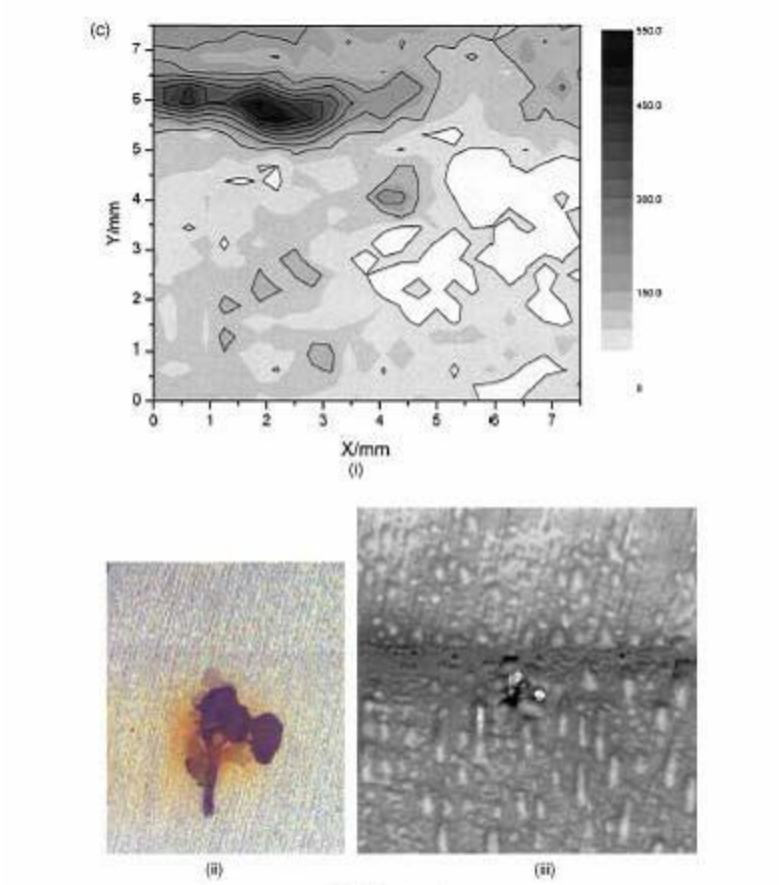

Fig. 9 (*continued*)

in the SKP results. We believe the reduction reaction to be conversion of red rust to magnetite [18], e.g.

$$Fe^{2+} + 8FeOOH + 2e^- = 3Fe_3O_4 + 4H_2O \quad (3)$$

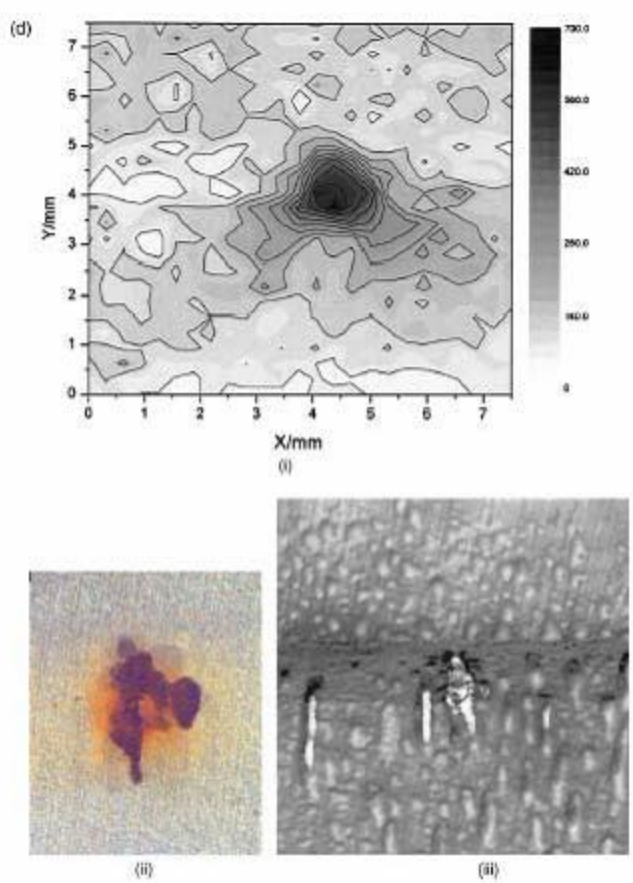

Fig. 9 (*continued*)

Stratmann [19] discovered that the potential at which reaction (3) can occur is between 0 and −400 mV SHE, depending on Fe^{2+} concentration and pH. This is in keeping with values of between −290 and −380 mV, measured during the test. The colour change of the corrosion products observed in the optical micrographs, from red to black, is consistent with this model.

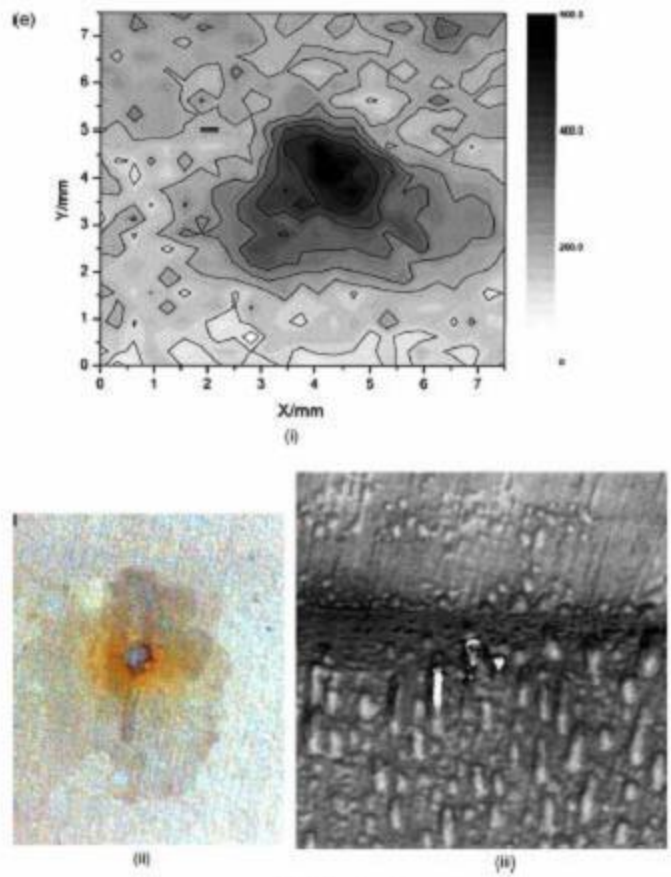

Fig. 9 (*continued*)

Hepburn [15] carried out low frequency ac impedance measurements on epoxy coated mild steel. She observed a Warburg impedance after a period of immersion in sodium sulphate solution, indicating diffusion control, but when the specimen was transferred to 0.1 M citric acid solution, which complexed the corrosion products and unplugged the pores, the Warburg impedance had disappeared. Charge transfer

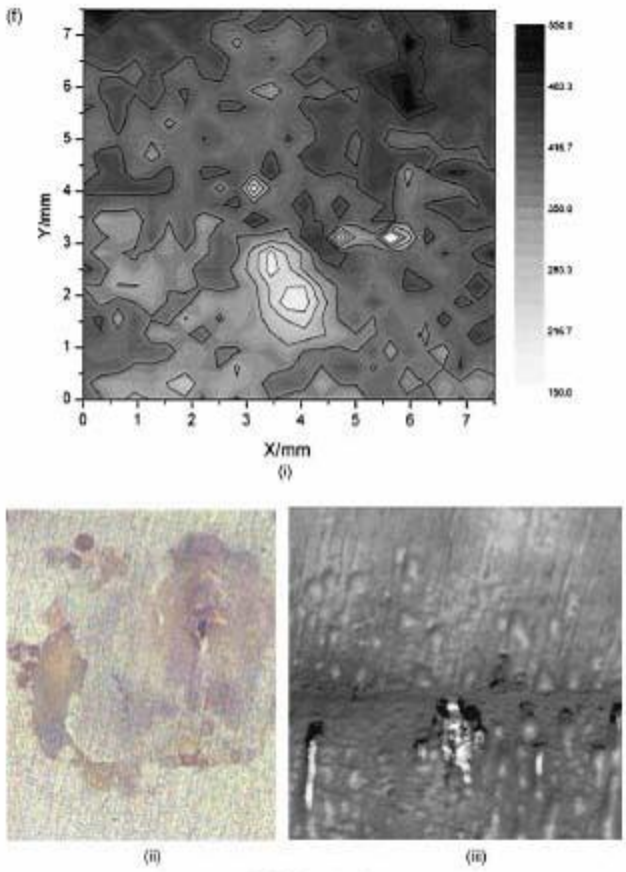

Fig. 9 (*continued*)

of corrosion reactions at the base of pores now controlled the low frequency impedance and a semi-circle is seen again.

Hepburn's findings are similar to our own EIS results shown in Fig. 10a–c. The impedance response in (c) is however represented best by a transmission line model. The physical model and equivalent circuit is shown in Fig. 11. The low frequency impedance response has contributions from charge transfer reactions

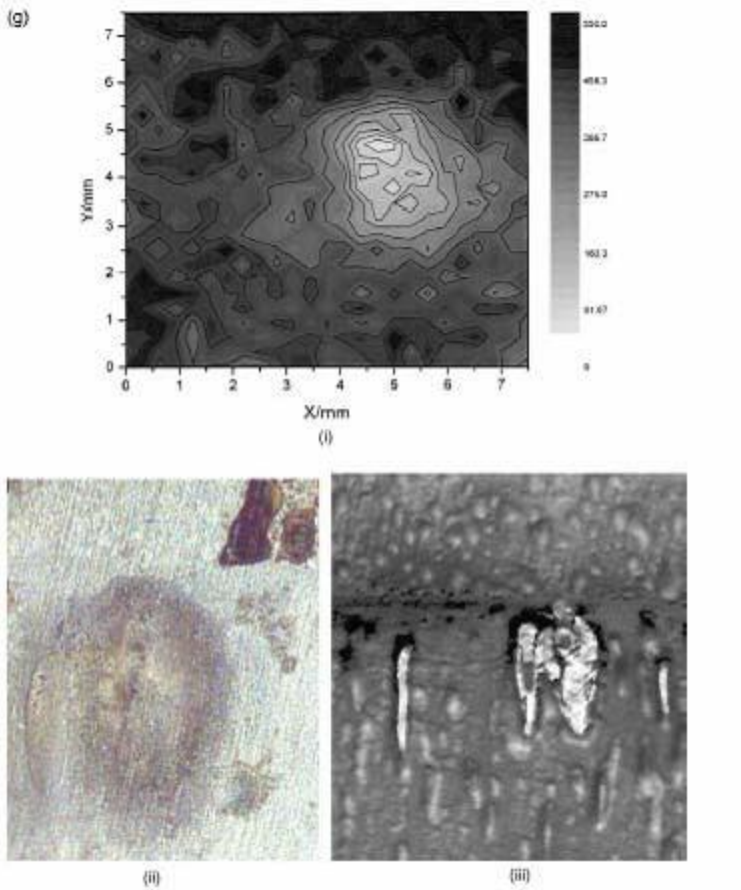

Fig. 9 (*continued*)

taking place all over the delaminated area as well as at the defect. The transmission line model used to fit the data used five distinct RC combinations, representing concentric regions around the defect. The impedance curves overlap on the Nyquist plot to give an accurate fit to the real data (Fig. 10), but it is difficult to

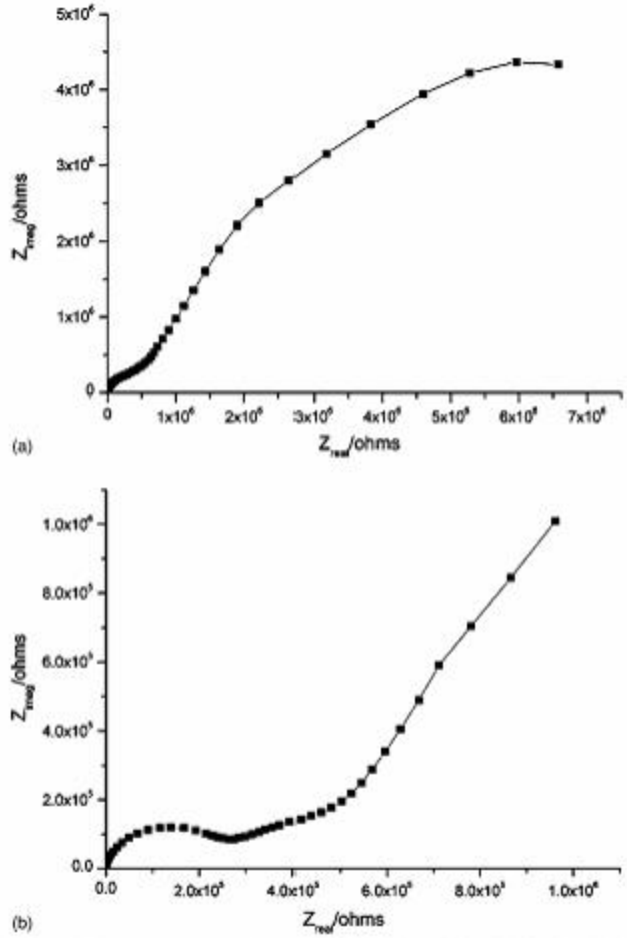

Fig. 10. Nyquist plots at various exposure times, (a) 5 h, (b) 20 h, (c) 170 h, (d) 50 h in 0.1 M citric acid.

extract values for the circuit parameters with any confidence. It should be noted that this good fit did not rely on the use of CPEs to model non-ideal capacitance—even for the coating.

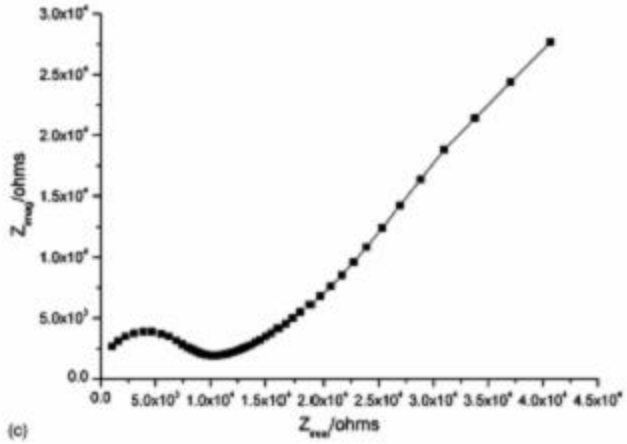

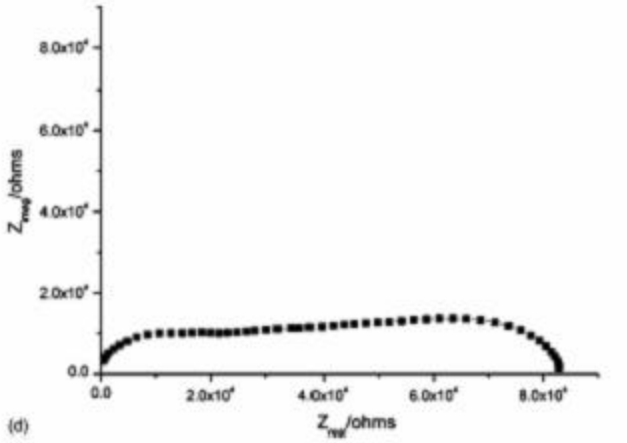

Fig. 10 (*continued*)

5. Conclusions

1. For this system, when a corrosion site becomes blocked with rust, new anodic sites are formed and the rust becomes the cathode reactant.

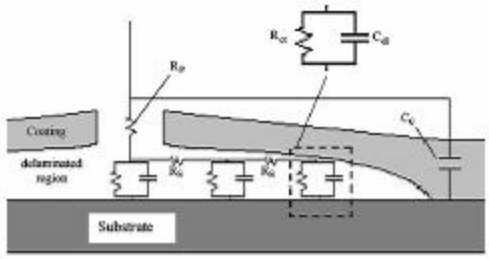

Fig. 11. Equivalent circuit for transmission line model and corresponding physical model.

2. An unblocked pore surrounded by a delaminated region is best modelled using a transmission line and does not require constant-phase elements.
3. The combination of SKP and SAM used alongside conventional optical microscopy and EIS are extremely powerful in analysing local behaviour in coating breakdown.

Acknowledgements

The authors are grateful to EPSRC and Crown Cork and Seal Company for provision of a CASE studentship and a research grant (EPSRC GR/N31887/01). We also thank Professor GDW Smith for provision of laboratory facilities and Mike Cochran and Paul Butler of Crown Cork and Seal Company for helpful discussions.

References

[1] P.J. Gay, J.O.C.C.A. 32 (352) (1949) 488.
[2] J.E.O. Mayne, J.O.C.C.A. 33 (361) (1950) 312.
[3] U. Steinsmo, E. Bardal, J. Electrochem. Soc. 136 (12) (1989) 3588.
[4] G. Meyer, W. Schwenk, Farbe Lack 85 (79) (1979).
[5] J.E.O. Mayne, J.O.C.C.A., 33(12) (1950) 538.
[6] A. Leng, H. Streckel, K. Hofmann, M. Stratmann, Corros. Sci. 41 (1999) 599.
[7] J.D. Crossen, J.M. Sykes, T. Zhai, G.A.D. Briggs, Faraday Discuss. (107) (1997) 417.
[8] W. Funke, Prog. Org. Coat. 9 (1981) 29.
[9] F.M. Geenen, J.H.W. de Wit, E.P.M. Van Westing, Prog. Org. Coat. 18 (1990) 299.
[10] R.R. Wiggle, A.G. Smith, J.V. Petrocelli, J. Paint Technol. 40 (174) (1968).
[11] R.W. Zurilla, in: H. Leidheiser (Ed.), Corrosion Control by Coatings, Science Press, Princeton, NJ, 1979, p. 243.
[12] http://www.ksi-germany.com/index.php?sp=2.
[13] F. Rossi, Rev. Sci. Instrum. 63 (9) (1992) 4174.
[14] I.D. Baikie, P.J. Estrup, Rev. Sci. Instrum. 69 (11) (1998) 3902.
[15] B.J. Hepburn, K.R. Gowers, J.D. Scantlebury, Br. Corros. J. 21 (2) (1986) 105.
[16] S.G. Yee, R.A. Oriani, M. Stratmann, J. Electrochem. Soc. 138 (1) (1991) 55.
[17] M. Doherty, J.M. Sykes, Unpublished work.
[18] U.R. Evans, C.J. Taylor, Corros. Sci. 12 (1972) 227.
[19] M. Stratmann, K. Bohnenkamp, H.J. Engell, Corros. Sci. 23 (9) (1983) 969.